Gamow-Teller transitions and proton-neutron pair correlation in $N = Z$ odd-odd p-shell nuclei

Hiroyuki Morita and Yoshiko Kanada-En'yo
Department of Physics, Kyoto University, Kyoto 606-8502, Japan
(Received 9 February 2017; revised manuscript received 11 August 2017; published 18 October 2017)

We have studied the Gamow-Teller (GT) transitions from $N = Z + 2$ neighbors to $N = Z$ odd-odd nuclei in the p-shell region by using isospin-projected and $\beta\gamma$-constraint antisymmetrized molecular dynamics combined with the generator coordinate method. The calculated GT transition strengths from 0^+1 states to 1^+0 states such as ^{6}He$(0_1{}^+1) \to {}^6$Li$(1_1{}^+0)$, ^{10}Be$(0_1{}^+1) \to {}^{10}$B$(1_1{}^+0)$, and ^{14}C$(0_1{}^+1) \to {}^{14}$N$(1_2{}^+0)$ exhaust more than 50% of the sum rule. These $N = Z + 2$ initial states and $N = Z$ odd-odd final states are found to dominantly have $S = 0, T = 1$ nn pairs and $S = 1, T = 0$ pn pairs, respectively. Based on the two-nucleon (NN) pair picture, we can understand the concentration of the GT strengths as the spin-isospin-flip transition $nn(S = 0, T = 1) \to pn(S = 1, T = 0)$ in LS coupling. The GT transition can be a good probe to identify the spin-isospin partner states with nn pairs and pn pairs of $N = Z + 2$ and $N = Z$ odd-odd nuclei, respectively.

DOI: 10.1103/PhysRevC.96.044318

I. INTRODUCTION

Proton and neutron (pn) correlation is one of the key phenomena to understand properties of $N = Z$ odd-odd nuclei (see Ref. [1] and references therein). In particular, a deuteron-like $T = 0$ pn pair plays an important role in low-lying states of light $N = Z$ odd-odd nuclei. Recently, a three-body model calculation of two nucleons with a doubly magic core nucleus was performed to study low-lying states of $N = Z$ odd-odd nuclei, and the result indicates that deuteron-like $S = 1, T = 0$ and dineutron-type $S = 0, T = 1$ pairs (LS-coupling pn pairs) are predominantly formed at the surface of double magic cores such as ^{16}O [2]. Moreover, in our previous work, we have studied pn correlation in ^{10}B and found the low-lying $T = 0$ and $T = 1$ states dominantly have the $S = 1, T = 0$ and $S = 0, T = 1$ pairs around a 2α core, respectively [3]. This indicates that LS coupling is better than jj coupling to understand pn pairs in light $N = Z$ odd-odd nuclei even though the LS-coupling pn pairs may change to jj-coupling pn pairs in heavy-mass systems because of the spin-orbit mean potential.

The Gamow-Teller transition is one of the useful observables to verify the LS-coupling pn pairs because it is sensitive to the spin-isospin configuration. For light $N = Z$ odd-odd nuclei, the GT operator flips nucleon spins and isospins of a pair and changes the dineutron-type nn pair to the deuteron-like pn pair. Similarly to the GT transition, the $M1$ transitions are analyzed to study spin-flip phenomena in $N = Z$ odd-odd nuclei, as done in Refs. [4,5] with shell model calculations for ^{10}B. However, one of the merits of the GT transition is that it is completely free from orbital contributions, which is different from the $M1$ transition. Moreover, if a system has two nucleons around a spin-isospin saturated core, collectivity of the proton-neutron pair can be probed by the ratio of the GT transition to the sum rule value. The spin-isospin-flip phenomena of pn pairs are different from so-called Gamow-Teller giant resonances which are contributed by collectivity of the excess neutrons. Recently, the super-allowed GT transitions in the low-energy region have been observed and discussed in relation to the pn correlations [6]. The LS-coupling pn pairs may play an important role in the low-energy superallowed GT transitions.

Although proton-neutron pairing correlations in medium and heavy mass $N = Z$ odd-odd nuclei have been discussed in jj coupling with mean field approaches [7–11], there are few theoretical works on study of LS-coupling pn pairs in light $N = Z$ odd-odd nuclei. For GT transitions in light nuclei, shell-model approaches [4,12–15] have been also applied, but they do not focus on descriptions of the collective excitation such as the spatial developments of the NN pairs and nuclear clusterizations, which are significant in particular in light nuclei. To extract information of NN pairs in light nuclei from the spin-isospin-flip phenomena, it is necessary to perform a systematic study of the GT transitions for ground and excited states while dealing with such collective excitations.

The authors have constructed a new framework, isospin-projected $\beta\gamma$-constraint antisymmetrized molecular dynamics ($T\beta\gamma$-AMD), which is useful for description of a pn pair in deformed or clustered systems [3]. In this paper, we investigate the GT transitions and pn pairs in p-shell nuclei by applying $T\beta\gamma$-AMD to ^{6}Li, ^{10}B, and ^{14}N. We discuss strong GT transitions in terms of an LS-coupling NN pair and propose an interpretation of the initial and final states as spin-isospin partners. Particular attention is paid to the roles of nonzero intrinsic spin ($S = 1$) of the $T = 0$ pn pair and its coupling with the orbital angular momentum of the pn center-of-mass motion and that of core rotation.

The paper is organized as follows. We briefly explain our framework in Sec. II. We show the results of nuclear properties of energy spectra, $B(M1)$, $B(E2)$, and B(GT), in Sec. III. We discuss the strong GT transitions in terms of the LS-coupling NN pair in Sec. IV by analyzing the obtained wave functions. A summary and an outlook are given in Sec. V.

II. METHOD

A. $T\beta\gamma$-AMD

For $N = Z$ odd-odd nuclei, we apply $T\beta\gamma$-AMD [3] in order to deal with the pn pair formation as well as nuclear deformation and clustering. For $N = Z + 2$ nuclei, we use $\beta\gamma$-constraint AMD [16], which has been used for structure studies of light neutron-rich nuclei as well as $Z = N$ even-even nuclei. We here briefly explain the formulation of $T\beta\gamma$-AMD.

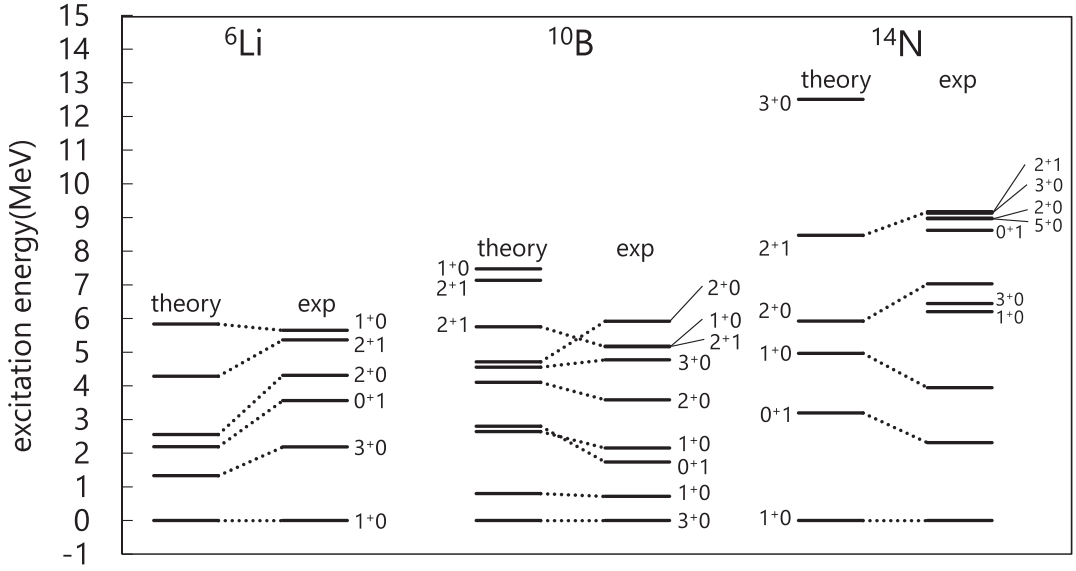

FIG. 1. Spectra of ^{6}Li, ^{10}B, and ^{14}N calculated by $T\beta\gamma$-AMD+GCM and those of the experimental data [22–24].

Details of the two methods, $T\beta\gamma$-AMD and $\beta\gamma$-AMD, are described in Refs. [3,16].

In the original framework of AMD, a basis wave function is written by a Slater determinant of Gaussian wave packets,

$$|\Phi(\beta,\gamma)\rangle = \mathcal{A}[|\phi_1\rangle|\phi_2\rangle\cdots|\phi_A\rangle], \tag{1}$$

$$|\phi_i\rangle = \left(\frac{2\nu}{\pi}\right)^{\frac{3}{4}} \exp\left[-\nu\left(\boldsymbol{r}_i - \frac{\boldsymbol{Z}_i}{\sqrt{\nu}}\right)^2\right]|\xi_i\rangle|\tau_i\rangle. \tag{2}$$

In the present work, we use $\nu = 0.235$ for p-shell nuclei as used in Refs. [16–21]. In $T\beta\gamma$-AMD, we perform parity and isospin ($^\pi T$) projections before variation as

$$|\Phi^{\pi T}(\beta,\gamma)\rangle = \hat{P}^\pi \hat{P}^T|\Phi(\beta,\gamma)\rangle, \tag{3}$$

where $\hat{P}^\pi$ and $\hat{P}^T$ are the parity projection operator and isospin projection operator, respectively. For the $^\pi T$-projected AMD wave function, we perform energy variation under the constraint on quadrupole deformation parameters $\beta\gamma$ and obtain the optimum solution for each set of β and γ values. In order to obtain wave functions for the nth $J^\pi T$ state (denoted by $J^\pi_n T$), we superpose the angular momentum eigenstates projected from the obtained wave functions $|\Phi^{\pi T}(\beta_i,\gamma_i)\rangle$,

$$\left|J^\pi_n T; M\right\rangle = \sum_{iK} c^{iK}_n \hat{P}^J_{MK}|\Phi^{\pi T}(\beta_i,\gamma_i)\rangle, \tag{4}$$

where $\hat{P}^J_{MK}$ is the angular momentum projection operator. Here, the parameters β and γ are treated as generator coordinates in the generator coordinate method (GCM), and the K mixing is taken into account. We call this method $T\beta\gamma$-AMD+GCM.

B. Effective interactions

We use the Hamiltonian

$$H = K - K_{\rm cm} + V_{\rm c} + V_{LS} + V_{\rm Coulomb}, \tag{5}$$

where K is the kinetic energy, $K_{\rm cm}$ is the kinetic energy of the center of mass, and $V_{\rm c}$, V_{LS}, and $V_{\rm Coulomb}$ are the central, spin-orbit, and Coulomb forces, respectively. For the central and spin-orbit forces, we use the effective nucleon-nucleon (NN) forces; the same as those used for ^{10}B in the previous work [3]. Namely, we use the Volkov No. 2 force of the central force with the Majorana exchange parameter $m = 0.6$ and the G3RS force of the spin-orbit force with the strength parameters $u_1 = -u_2 = 1300$ MeV.

For the Bartlett and Heisenberg parameters, b and h, of the Volkov No. 2 force, we use $b = h = 0.125$ for ^{6}Li, which reproduce the S-wave NN scattering lengths in the $T = 0$ and $T = 1$ channels. For ^{10}B and ^{14}N, we adopt a parametrization $b = h = 0.06$, phenomenologically modified so as to describe energy difference between the lowest $T = 0$ and $T = 1$ states in each nucleus. The parameters b and h control the ratio (f) of the central force in the $T = 0$ channel to that in the $T = 1$ channel. The present choices, $b = h = 0.125$ and $b = h = 0.06$, give the ratios $f = 1.67$ and 1.27, respectively. The decrease of f is consistent with the naive expectation that the $T = 0$ interaction is somewhat suppressed by a nuclear medium effect. We should comment that, even though relative position between $T = 1$ and $T = 0$ spectra is sensitive to b and h, we obtain almost the same energy spectra in each isospin channel and also qualitatively similar results for structure properties of ^{10}B and ^{14}N in the cases of $b = h = 0.125$ and $b = h = 0.06$.

III. RESULTS

A. $T\beta\gamma$-AMD results

Calculated energy spectra of ^{6}Li, ^{10}B, and ^{14}N obtained by $T\beta\gamma$-AMD+GCM are shown in Fig. 1 compared with experimental spectra. The present calculation reasonably reproduces the low-energy spectra of these nuclei.

The calculated binding energies, magnetic dipole moments (μ), electric quadrupole moments (Q), and $E2$ and $M1$ transition strengths of ^{6}Li, ^{10}B, and ^{14}N are listed in Table I together with experimental data. The present calculation

TABLE I. Binding energies, μ and Q moments, and $M1$ and $E2$ transition strengths of ^{6}Li, ^{10}B, and ^{14}N. The calculated values obtained by $T\beta\gamma$-AMD+GCM are shown. For comparison, the values calculated by shell models are shown. Experimental data are taken from [22–24].

Observable	$T\beta\gamma$-AMD+GCM	SM	Expt.
^{6}Li			
$\|E(1_1^+0)\|$ (MeV)	29.55	31.036 [13]	31.994
$\mu(1_1^+0)$ (μ_N)	0.87	0.840 [13]	0.82205
$Q(1_1^+0)$ (fm^2)	0.09	−0.025 [13]	−0.0818(17)
$B(E2;3_1^+0 \to 1_1^+0)$	3.79	3.040 [13]	10.7(8)
$B(M1;0_1^+1 \to 1_1^+0)$	13.73	15.374 [13]	15.4(3)
$B(E2;2_1^+0 \to 1_1^+0)$	5.15	3.129 [13]	4.4(23)
$B(M1;2_1^+1 \to 1_1^+0)$	0.01	0.113 [13]	0.15(3)
^{10}B			
$\|E(3_1^+0)\|$ (MeV)	60.35	60.567 [13]	64.751
$\mu(3_1^+0)$ (μ_N)	1.83	1.847 [13]	1.8006
$\mu(1_1^+0)$ (μ_N)	0.84	0.802 [13]	0.63(12)
$Q(3_1^+0)$ (fm^2)	8.45	5.682 [13]	8.47(6)
$B(E2;1_1^+0 \to 3_1^+0)$	4.03	1.959 [13]	4.147(20)
$B(M1;0_1^+1 \to 1_1^+0)$	14.98	14.3 [5]	7.5(34)
$B(M1;1_2^+0 \to 0_1^+1)$	0.05	0.09 [4]	0.192(20)
$B(E2;1_2^+0 \to 1_1^+0)$	9.23	3.384 [13]	15.6(17)
$B(E2;1_2^+0 \to 3_1^+0)$	2.02	1.010 [13]	1.70(20)
$B(E2;2_1^+0 \to 3_1^+0)$	0.34	1.0 [4]	1.2(4)
$B(E2;3_2^+0 \to 1_1^+0)$	10.56	3.543 [13]	19.7(17)
$B(M1;2_1^+1 \to 2_1^+0)$	1.84	3.1 [4]	2.52(68)
$B(M1;2_1^+1 \to 1_2^+0)$	2.60	2.0 [4]	3.06(82)
$B(M1;2_1^+1 \to 1_1^+0)$	0.31	0.2 [4]	0.32(9)
^{14}N			
$\|E(1_1^+0)\|$ (MeV)	108.60	108.41 [12]	104.66
$\mu(1_1^+0)$ (μ_N)	0.34	0.347 [12]	0.40376
$Q(1_1^+0)$ (fm^2)	0.53	1.19 [12]	1.93(8)
$B(M1;0_1^+1 \to 1_1^+0)$	0.76	0.29 [12]	0.047(2)
$B(M1;1_2^+0 \to 0_1^+1)$	3.72	–	1.8(11)
$B(E2;1_2^+0 \to 1_1^+0)$	3.25	–	4.4(24)
$B(E2;2_1^+0 \to 1_1^+0)$	2.95	–	3.6(8)
$B(M1;2_1^+1 \to 2_1^+0)$	4.65	–	1.7(3)
$B(M1;2_1^+1 \to 1_1^+0)$	0.00	–	0.59(4)

quantitatively or qualitatively reproduces the experimental data of these properties.

μ moments and $B(M1)$ as well as the GT transition strengths are observables that sensitively reflect spin configurations. The calculated μ moments of the ground states, ^{6}Li(1_1^+0), ^{10}B(3_1^+0), and ^{14}N(1_1^+0), and that of ^{10}B(1_1^+0) agree well with the experimental data. For the $M1$ transition in ^{6}Li, the remarkably large $B(M1;0_1^+1 \to 1_1^+0)$ is well reproduced by the calculation. For ^{10}B, the $M1$ transitions between $T = 1$ and $T = 0$ states are qualitatively described although quantitative reproduction is not satisfactory in the present calculation. For ^{14}N, the present calculation describes the general trend of the relatively strong $M1$ transitions for $1_2^+0 \to 0_1^+1$ and $2_1^+1 \to 2_1^+0$ compared with those for other transitions.

TABLE II. Gamow-Teller transition strengths of ^{6}He $\to$ ^{6}Li, ^{10}Be $\to$ ^{10}B, and ^{14}C $\to$ ^{14}N. Calculated values of B(GT) defined in Eq. (6) are shown. For comparison, the B(GT) values calculated by shell models are shown. Experimental data are taken from [24,29–32]. The values in the parentheses are for the mirror transitions.

Initial $\to$ final	$T\beta\gamma$-AMD+GCM	SM	Expt.
^{6}He $\to$ ^{6}Li			
$0_1^+1 \to 1_1^+0$	5.31	5.213 [13]	4.809(8)
$0_1^+1 \to 1_2^+0$	0.00		
$2_1^+1 \to 1_1^+0$	0.01		
$2_1^+1 \to 3_1^+0$	0.97		
$2_1^+1 \to 2_1^+0$	1.00		
$2_1^+1 \to 1_2^+0$	1.10		
^{10}Be $\to$ ^{10}B			
$0_1^+1 \to 1_1^+0$	4.95	(4.331) [13]	(3.5101(57))
$0_1^+1 \to 1_2^+0$	0.15	(0.497) [14]	(<0.813)
$0_1^+1 \to 1_3^+0$	0.00		
$2_1^+1 \to 3_1^+0$	0.63	0.092 [13]	0.11(4)
$2_1^+1 \to 1_1^+0$	0.06		
$2_1^+1 \to 1_2^+0$	0.81		
$2_1^+1 \to 2_1^+0$	0.77		
$2_1^+1 \to 3_2^+0$	1.71		
$2_1^+1 \to 1_3^+0$	0.26		
$2_1^+1 \to 2_2^+0$	0.86		
$2_2^+1 \to 3_1^+0$	1.54	1.807 [13]	1.3(2)
$2_2^+1 \to 1_1^+0$	0.01		
$2_2^+1 \to 1_2^+0$	0.23		
$2_2^+1 \to 2_1^+0$	0.71		
$2_2^+1 \to 3_2^+0$	0.26		
$2_2^+1 \to 1_3^+0$	0.82		
$2_2^+1 \to 2_2^+0$	0.79		
^{14}C $\to$ ^{14}N			
$0_1^+1 \to 1_1^+0$	0.30	0.0175 [14] 1.69×10^{-4} [12]	$3.53(2) \times 10^{-6}$
$0_1^+1 \to 1_2^+0$	4.32	(4.445) [14]	2.76(11)
$2_1^+1 \to 1_1^+0$	1.13		0.27
$2_1^+1 \to 2_1^+0$	1.77		
$2_1^+1 \to 3_1^+0$	2.35		

For ^{10}B, the calculated Q moment and $B(E2;3_2^+0 \to 1_1^+0)$ are large because of the prolate deformation and this is consistent with the experimental data. The prolate deformation of ^{10}B is caused by formation of a 2α core as shown later.

In order to calculate GT transition strengths, we apply $\beta\gamma$-AMD and obtain wave functions for the ground and excited states of ^{6}He, ^{10}Be, and ^{14}C, which are isobaric analog states of $T = 1$ states of ^{6}Li, ^{10}B, and ^{14}N. Table II shows the calculated B(GT):

$$B(\mathrm{GT}) = \frac{1}{2J_i+1}\left|\langle J_f \| \sum_i \boldsymbol{\sigma}^i \tau_\pm^i \| J_i\rangle\right|^2. \quad (6)$$

In the present paper, we define B(GT) by matrix elements of the spin and isospin operators without the factor $(g_A/g_V)^2$. For all low-lying states of ^{6}Li, ^{10}B, and ^{14}N, we find $T = 0$

states that have strong GT transitions with large percentages of the sum rule $\sum B(\mathrm{GT}) = 3(N-Z) = 6$. These final states in $Z = N$ odd-odd nuclei can be regarded as "spin-isospin partners" of the corresponding $T = 1$ initial states because they are approximately spin-isospin-flipped states having spatial configurations similar to the initial states. The concept of the spin-isospin partners is an extension of the isobaric analog state (IAS) to the GT transition. The assignments of the spin-isospin partners in the following discussions are based on the calculated GT transition strengths and also spin and orbital configurations of NN pairs.

For ^{6}Li, the GT transition from the ground state ^{6}He($0_1{}^+1$) to $1_1{}^+0$ exhausts a large fraction of the sum rule, consistent with the experimental data, whereas that to $1_2{}^+0$ is weak. This fact indicates that the ground states of ^{6}Li and ^{6}He are almost ideal spin-isospin partners. For the GT transitions from the excited state, ^{6}He($2_1{}^+1$), we obtain strong transitions to $1_2{}^+0$, $2_1{}^+0$, and $3_1{}^+0$. The summation of B(GT) values for these three states is about 50% of the sum rule, and therefore these states are regarded as the set of spin-isospin partners with $J^\pi = \{1^+,2^+,3^+\}$ of the ^{6}He($2_1{}^+1$).

Also for ^{10}B, the GT transition strength from the ground state ^{10}Be($0_1{}^+1$) is concentrated to $1_1{}^+0$. For the GT transitions from the excited states ^{10}Be($2_1{}^+1$) and ^{10}Be($2_2{}^+1$), significant strengths are obtained for transitions to $1_2{}^+0$, $1_3{}^+0$, $2_1{}^+0$, $2_2{}^+0$, $3_1{}^+0$, and $3_2{}^+0$, which can be assigned to two sets of spin-isospin partners with $J^\pi = \{1^+,2^+,3^+\}$ of ^{10}Be($2_1{}^+1$) and ^{10}Be($2_2{}^+1$). In particular, the transitions from ^{10}Be($2_1{}^+1$) are significantly strong to $1_2{}^+0$ and $3_2{}^+0$, indicating that these states are regarded as spin-isospin partner states. In the transitions from ^{10}Be($2_2{}^+1$), the strengths to $1_3{}^+0$ and $3_1{}^+0$ are significantly large, hence these states can be assigned to the spin-isospin partners of ^{10}Be($2_2{}^+1$). For assignment of $J^\pi = 2^+$ states, the strengths $2_1{}^+1 \to 2_1{}^+0$, $2_1{}^+1 \to 2_2{}^+0$, $2_2{}^+1 \to 2_1{}^+0$, and $2_2{}^+1 \to 2_2{}^+0$ are comparable. It indicates that two $J^\pi = 2^+$ states corresponding to the partner states of ^{10}Be($2_1{}^+1$) and ^{10}Be($2_2{}^+1$) are strongly mixed with each other.

For ^{14}N, the strongest GT transition from the ground state ^{14}C($0_1{}^+1$) is obtained for $1_2{}^+0$, consistent with the experimental data. It indicates that not $1_1{}^+0$ but $1_2{}^+0$ of ^{14}N is the spin-isospin partner in the $A = 14$ systems. Compared with the dominant transition $0_1{}^+1 \to 1_2{}^+0$, the calculated transition $0_1{}^+1 \to 1_1{}^+0$ is relatively minor but it does not reproduce the anomalously small value of the experimental datum. Tensor and three-body forces may be necessary, as discussed by many works [12,15,25–28], in order to obtain the very small B(GT) for the $0_1{}^+1 \to 1_1{}^+0$ transition. Those effects are not included in the present calculation. For the transitions from the first excited state $2_1{}^+1$, strengths to $1_1{}^+0$, $2_1{}^+0$, and $3_1{}^+0$ are significant, and the sum of them exhausts more than 80% of the sum rule; thus, these states are regarded as the spin-isospin partners.

B. Comparison with shell model results

For comparison, we also list the shell model results of nuclear properties and $E2$ transition strengths in Table I, and those of GT transition strengths in Table II. The theoretical data of shell models are taken from Refs. [4,5] for traditional shell model calculations, from Ref. [13] for the no-core shell model (NCSM) calculation in the $6\hbar\omega$ model space using the Argonne V8′ nucleon-nucleon NN potential combined with the Tucson-Melbourne TM′8(99) three-nucleon interaction, and from Ref. [12] for the NCSM using the nuclear interactions of two-body and three-body forces derived from chiral perturbation theory. It should be noted that a coupling constant for the three-body forces used in Ref. [12] is tuned to fit the anomalously small B(GT; ^{14}C($0_1{}^+1$) $\to$ ^{14}N($1_1{}^+0$)).

For ^{10}B, the $Q(3_1{}^+0)$ moment and $E2$ transition strengths are significantly improved by $T\beta\gamma$-AMD compared with the shell model calculations, because ^{10}B is a well deformed nucleus with a developed 2α cluster. The shell models generally underestimate the experimental data of the Q moment and $B(E2)$. For instance, they give about factor 2 smaller values than the experimental data for $B(E2; 1_1{}^+0 \to 3_1{}^+0)$, $B(E2; 1_2{}^+0 \to 1_1{}^+0)$, $B(E2; 1_2{}^+0 \to 3_1{}^+0)$, and $B(E2; 3_2{}^+0 \to 1_1{}^+0)$, meaning that the $6\hbar\omega$ model space is still insufficient to describe the well deformed structure induced by the spatially developed 2α core and the pn pair structure.

In general, spatial development of a cluster structure involves higher-shell components. In order to demonstrate significant higher-shell components in the obtained ^{10}B wave functions because of the developed cluster structure, we show in Table III the expectation values of the harmonic oscillator quanta $\mathcal{N}_{\hbar\omega} = \sum_i a_i^\dagger a_i$. Here, $a_i^\dagger$ and a_i are the creation and annihilation operators of a harmonic oscillator with width parameter $\nu = 0.235$ fm^{-2}. The difference $\Delta\mathcal{N}_{\hbar\omega} = \langle\mathcal{N}_{\hbar\omega}\rangle - \mathcal{N}_{\hbar\omega,\mathrm{min}}$ from the minimum values for the $0\hbar\omega$ configurations are listed. Nonzero $\Delta\mathcal{N}_{\hbar\omega}$ values indicate significant mixing of higher shell components beyond the p shell because of the spatial development of two-nucleon pairs and α particles (see Sec. IV A). In particular, $A = 10$ nuclei show significant enhancement of $\Delta\mathcal{N}_{\hbar\omega}$ compared with $A = 6,14$ systems because of spatial development of the 2α cluster in addition to that of two-nucleon pairs. Indeed, the $\Delta\mathcal{N}_{\hbar\omega}$ of ^{10}B($1_1{}^+0$) is larger than those of ^{6}Li($1_1{}^+0$) and ^{10}N($1_1{}^+0$) since ^{10}B contains the strongly deformed 2α core. In the ^{10}B levels, $\Delta\mathcal{N}_{\hbar\omega}$ of $1_1{}^+0$ is larger than that of $3_1{}^+0$, reflecting the spatially developed pn pair from the 2α core in ^{10}B($1_1{}^+0$). This result indicates that higher-shell components are necessary to describe the spatially developed NN pairs and α particles, as expected.

For $A = 6$ and $A = 14$ nuclei with spherical cores, on the other hand, most of the $T\beta\gamma$-AMD values for the nuclear moments and the transition strengths correspond well to those of the shell model calculations. For ^{6}Li, there is slight difference in the nuclear moments, and the electric transition strengths show almost same tendency. In detail, the large experimental $B(E2; 3_1{}^+0 \to 1_1{}^+0)$ datum is underestimated for our model and the shell models and the other transition data are well reproduced qualitatively in both methods. For ^{14}N, binding energies and magnetic moments are almost consistent between two calculations. The quadrupole moments and $B(M1; 0_1{}^+1 \to 1_1{}^+0)$ are somewhat worse in our calculation than the shell models.

TABLE III. Expectation values of the squared intrinsic spin and orbital angular momentum ($\langle \boldsymbol{S}^2 \rangle$ and $\langle \boldsymbol{L}^2 \rangle$) for ^{6}Li, ^{10}B, and ^{14}N obtained by $T\beta\gamma$-AMD+GCM and ^{6}He, ^{10}Be, and ^{14}C obtained by $\beta\gamma$-AMD+GCM. For harmonic oscillator quanta, values of the difference $\Delta\mathcal{N}_{\hbar\omega} = \langle \mathcal{N}_{\hbar\omega} \rangle - \mathcal{N}_{\hbar\omega,\min}$ from the minimum values for the $0\hbar\omega$ configurations are listed. $\mathcal{N}_{\hbar\omega,\min}$ for $A = 6,10,14$ nuclei are $\mathcal{N}_{\hbar\omega,\min} = 2,6,10$, respectively.

$N = Z + 2$					$N = Z$ odd-odd								
Nuclide	$J_n^\pi T$	$\langle \boldsymbol{S}^2 \rangle$	$\langle \boldsymbol{L}^2 \rangle$	$\Delta\mathcal{N}_{\hbar\omega}$	Nuclide	$J_n^\pi T$	$\langle \boldsymbol{S}^2 \rangle$	$\langle \boldsymbol{L}^2 \rangle$	$\Delta\mathcal{N}_{\hbar\omega}$	$J_n^\pi T$	$\langle \boldsymbol{S}^2 \rangle$	$\langle \boldsymbol{L}^2 \rangle$	$\Delta\mathcal{N}_{\hbar\omega}$
^{6}He	0_1^+1	0.12	0.12	1.45	^{6}Li	0_1^+1	0.12	0.12	1.71	1_1^+0	1.97	0.06	0.89
	2_1^+1	0.19	5.65	1.63		2_1^+1	0.20	5.64	1.91	1_2^+0	1.90	5.75	1.20
										2_1^+0	2.00	5.99	1.97
										3_1^+0	2.01	6.01	0.70
^{10}Be	0_1^+1	0.34	0.34	1.90	^{10}B	0_1^+1	0.28	0.28	1.97	1_1^+0	1.94	0.35	2.37
	2_1^+1	0.30	6.00	1.94		2_1^+1	0.27	6.04	1.90	1_2^+0	1.92	5.43	1.77
										2_1^+0	2.02	6.49	2.03
										3_2^+0	1.97	7.53	2.21
	2_2^+1	0.12	6.11	2.08		2_2^+1	0.10	6.08	2.07	1_3^+0	1.99	5.94	3.03
										2_2^+0	2.02	6.61	2.44
										3_1^+0	2.05	7.15	1.46
^{14}C	0_1^+1	0.55	0.55	0.50	^{14}N	0_1^+1	0.61	0.61	0.70	1_2^+0	1.94	0.44	0.96
	2_1^+1	0.19	5.79	0.74		2_1^+1	0.21	5.83	0.88	1_1^+0	1.89	5.56	0.45
										2_1^+0	2.01	6.07	0.80
										3_1^+0	2.02	6.22	1.32

The Gamow-Teller transition strengths of the shell model [12,14] are compared with the present calculations as well as the experimental data in Table II. The shell model values are comprehensively comparable with the $T\beta\gamma$-AMD values except for $B(\mathrm{GT}; 0_1^+1 \to 1_1^+0)$ of $^{14}\mathrm{C} \to {}^{14}\mathrm{N}$. Although the present calculation reproduces the trend of the GT transition for $0_1^+1 \to 1_2^+0$ more strongly than that for $0_1^+1 \to 1_1^+0$, it fails to quantitatively reproduce the anomalously small $B(\mathrm{GT}; 0_1^+1 \to 1_1^+0)$.

In the comparison of nuclear properties between the shell model and the $T\beta\gamma$-AMD calculations, we have found that the present calculation describes the spatial development of 2α particles and NN pairs in ^{10}B better than the shell model calculations. Nevertheless, for many of spin(-isospin) observables such as the $M1$ and GT transitions, the results calculated with $T\beta\gamma$-AMD correspond well to the shell model results. It may indicate that major-shell spin configurations, which dominantly contribute to these observables, are similar to each other in the $T\beta\gamma$-AMD and shell model calculations.

IV. DISCUSSION

In the previous section, we assigned the spin-isospin partners from the strong GT transitions based on the NN pair picture. In this section, we discuss detailed features of NN pairs in the spin-isospin-partner states and show that the spin-isospin-partner states can be simply understood by NN pairs moving around α and 2α cores and two-hole pairs in the ^{16}O core.

A. Intrinsic structure and spatial distribution of a proton-neutron pair

In the obtained wave functions for the $A = 6$, $A = 10$, and $A = 14$ systems, NN pairs are found to be formed around α, 2α, and ^{12}C cores, respectively. In order to see the spatial distribution of the $S = 1, T = 0$ and $S = 0, T = 1$ NN pairs in the spin-isospin partners, we calculate two-particle density $\rho_{ST}(\boldsymbol{r})$ at the identical point $\boldsymbol{r}$ in the intrinsic states, defined as

$$\rho_{ST}(\boldsymbol{r}) = \frac{\langle \Phi^T(\beta,\gamma) \,|\, \hat{\rho}_{ST}(\boldsymbol{r}) \,|\, \Phi^T(\beta,\gamma) \rangle}{\langle \Phi^T(\beta,\gamma) \,|\, \Phi^T(\beta,\gamma) \rangle}, \tag{7}$$

$$\hat{\rho}_{ST}(\boldsymbol{r}) \equiv \sum_{ij} \hat{P}_{ij}^S \hat{P}_{ij}^T \delta(\boldsymbol{r} - \hat{\boldsymbol{r}}_i)\delta(\boldsymbol{r} - \hat{\boldsymbol{r}}_j), \tag{8}$$

where $\hat{P}_{ij}^S$ and $\hat{P}_{ij}^T$ are the spin and isospin projection operators for two particles. We define the two-nucleon-pair density $\rho_{NN}(\boldsymbol{r}) \equiv \rho_{10}(\boldsymbol{r}) - \rho_{01}(\boldsymbol{r})$ to cancel NN pair contributions from α clusters which contain the same numbers of $S = 1, T = 0$ NN pairs as those of $S = 0, T = 1$ NN pairs. With this definition, positive (negative) regions of $\rho_{NN}(\boldsymbol{r})$ indicate $S = 1, T = 0$ ($S = 0, T = 1$) pn-pair distributions in $T = 0$ ($T = 1$) states. In Fig. 2, we show the two-nucleon-pair density $\rho_{NN}(\boldsymbol{r})$ together with the one-body density distribution in the single Slater-determinant state which has the largest overlap in the $\beta\gamma$ plane with the wave function for each of the ground 0_1^+1 states of ^{6}He, ^{10}Be, and ^{14}C and their spin-isospin partner 1^+0 states of the $N = Z$ odd-odd nuclei.

In the ground state of ^{6}Li, an α particle and a $T = 0$ pn pair are formed as seen in Fig. 2(d). The pn pair spatially develops away from the α core and it shows deuteron-like nature. Also in ^{6}He, the two-neutron pair appears around an α core [Fig. 2(a)]. The spatial distribution of the nn pair density in ^{6}He is quite similar to that of the pn pair density in ^{6}Li, indicating that these states are good spin-isospin partner states, in which the two-nucleon spin S and isospin T flip from $nn(T = 1, S = 0)$ in ^{6}He to $pn(T = 0, S = 1)$ in ^{6}Li.

In $^{14}\mathrm{N}(1_2^+0)$ [see Fig. 2(f)], a $T = 0$ pn pair is distributed at the surface of the oblately deformed ^{12}C core. In $^{14}\mathrm{C}(0_1^+1)$,

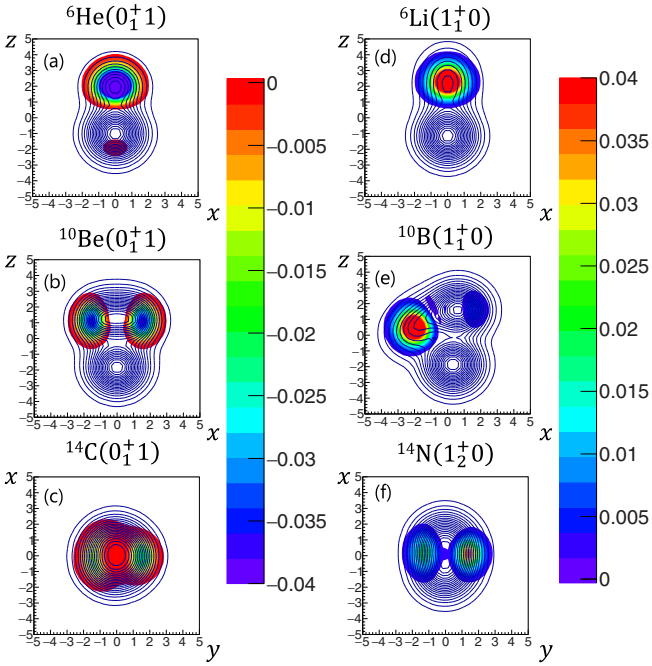

FIG. 2. The colored contours show two-nucleon-pair density $\rho_{NN}(\boldsymbol{r})$ of (a)^{6}He(0_1^+1), (b)^{10}Be(0_1^+1), (c)^{14}C(0_1^+1), (d)^{6}Li(1_1^+0), (e)^{10}B(1_1^+0), and (f)^{14}N(1_2^+0). The blue contours show the one-body density distribution $\rho(\boldsymbol{r})$.

the nn pair density around the ^{12}C core shows a distribution similar to the pn pair in ^{14}N(1_2^+0). The NN pairs in ^{14}N(1_2^+0) and ^{14}C(0_1^+1) show no spatial development and dominantly consist of p-orbit nucleons. If we consider a ^{16}O core, these states can be understood as two-hole pairs in the p shell of the ^{16}O core.

In ^{10}B(1_1^+0), the deformation on β and γ is realized as formation of the 2α clusters. In the total density in Fig. 2(e), we can find one α particle near the point $(x,z) = (0.0, 2.0)$ (fm) and the other near $(0.0, -2.0)$ (fm). It indicates that the prolate deformation is caused by development of the 2α cluster with an intercluster distance about 4.0 fm. This is the major reason why our model gives as large a Q moment as the experimental data. This is one of the advantages of the present model, $T\beta\gamma$-AMD, making it superior to shell models which do not explicitly include the clustering effect.

A $T = 0$ pn pair is also formed around the 2α cluster [see Fig. 2(e)]. The $T = 0$ pn pair develops away from the 2α core similarly to ^{6}Li, whereas the nn pair in ^{10}Be(0_1^+1) is not so developed spatially but is distributed at the nuclear surface, showing a feature of two p-orbit neutrons [Fig. 2(b)]. Although the single Slater-determinant state with the largest overlap for ^{10}Be(0_1^+1) shows less development of the two-nucleon pair than that for ^{10}B(1_1^+0), in the $\beta\gamma$-AMD+GCM result the spatially developed nn pair components are largely mixed because the two-neutron pair can move away from the 2α core along a plateau toward a finite γ region in the $J^\pi = 0^+$ energy surface of ^{10}Be [3]. As a result, the nn pair distribution in ^{10}Be(0_1^+1) has a large overlap with the pn pair distribution in ^{10}B, and therefore these states have a strong GT transition and are regarded as the partner states.

Let us discuss spatial development of the NN pairs with A increasing in the $A = 6$, $A = 10$, and $A = 14$ systems. In the 0^+1 ground states of $N = Z + 2$ nuclei, the nn pair is mostly developed spatially in the $A = 6$ nucleus and comes down to the p-shell configurations in $A = 10$ and $A = 14$ nuclei with increasing mass number. In the partner 1^+ states of the $N = Z$ odd-odd nuclei, the spatially developed $T = 0$ pn pair is prominent in the $A = 6$ nucleus and it more or less weakens but still remains even in the $A = 10$ nucleus, and finally comes down to the p-shell configuration in the $A = 14$ nucleus. This result reflects the feature that the $T = 0$ pn pairs in $N = Z$ odd-odd nuclei are more robust than nn pairs in $N = Z + 2$ nuclei. Indeed, the $T = 0$ pn pairs are described well by the LS-coupling pairs, whereas nn pairs are somewhat broken from the LS-coupling pairs and contain mixing of jj-coupling components, in particular in the $A = 10$ and $A = 14$ nuclei, as shown later in analysis of spin configurations.

B. LS-coupling pn pairs and spin-isospin partners

To quantitatively discuss the spin and orbital configurations, we show the expectation values of the squared intrinsic spin and orbital angular momentum ($\langle \boldsymbol{S}^2 \rangle$ and $\langle \boldsymbol{L}^2 \rangle$) in Table III. Note that $\langle \boldsymbol{S}^2 \rangle$ approximately indicates the expectation value of the squared intrinsic spin of a NN pair around a core because core contribution is minor in the present case: the obtained states of the $A = 6$ and $A = 10$ nuclei are understood by two particles around $S = 0$ cores such as α and 2α and those of the $A = 14$ nuclei are approximately interpreted as two-hole states of ^{16}O. $T = 1$ states of the $N = Z$ odd-odd nuclei have almost same expectation values as those of the $N = Z + 2$ nuclei because they are isobaric analog states. In this section, we discuss spin and orbital configurations based on the picture of two-nucleon (two-hole) pairs around cores.

In the following discussion, we focus on the LS-coupling NN pairs, in particular, those around the 2α core in $A = 10$ nuclei. Note that the terminology "LS-coupling" here is used for the coupling of intrinsic spin S_{NN} and its orbital-angular momentum L_{NN} of two nucleons in the spatially developed NN pairs, but it is different from the "LS-coupling scheme" of the shell model, which are often used for the orbital-angular momentum and intrinsic spin coupling of major-shell nucleons. Even though a LS-coupling NN pair in the major shell around a spherical core is a special case equivalent to two nucleons in the "LS-coupling scheme" of the shell model, in the case of the LS-coupling NN pairs around deformed cores, the total angular momentum J is constructed by the coupling of S_{NN} and L_{NN} of the pair, and also the orbital angular momentum $L_{\rm core}$ from collective rotation of the core. This picture of the LS-coupling NN pairs around core nuclei is useful in systematical discussion of properties of the NN pairs in $A = 6$, $A = 10$, and $A = 14$ nuclei to figure out the role of the NN pairs in $A = 10$ nuclei with the developed 2α cluster.

In the obtained states of the $A = 6$, $A = 10$, and $A = 14$ nuclei, the spin expectation values of $T = 0$ ($T = 1$) states are close to the value $\langle \boldsymbol{S}^2 \rangle = 2$ ($\langle \boldsymbol{S}^2 \rangle = 0$) for $S = 1$ ($S = 0$) component. It implies that LS-coupling NN pairs are formed

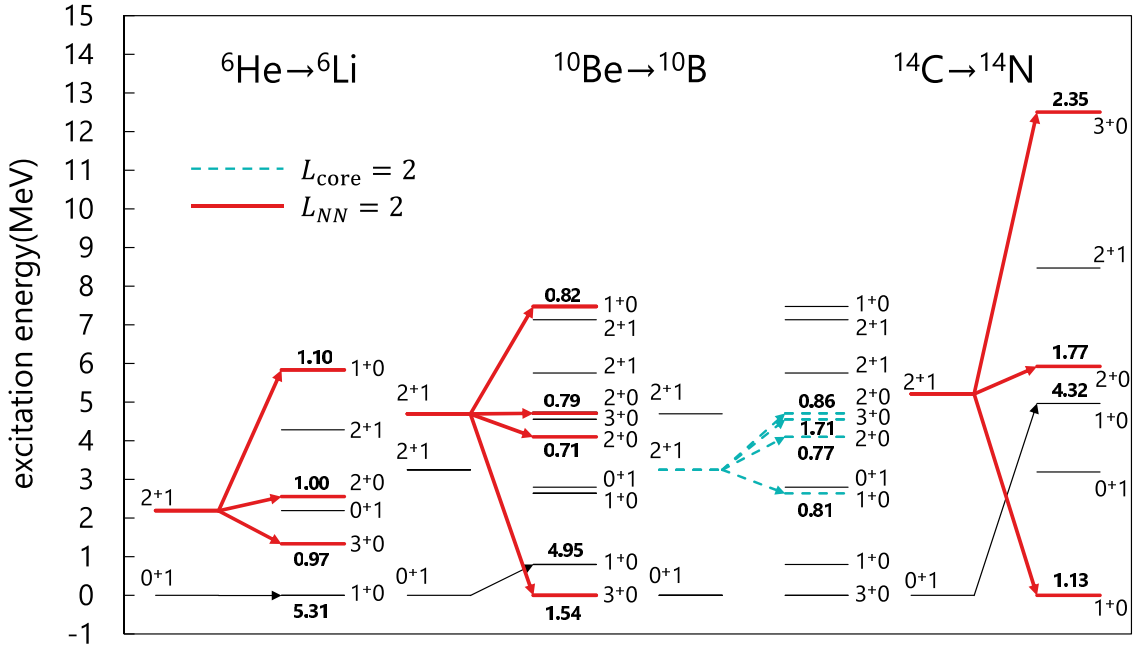

FIG. 3. GT transitions ^{6}He → ^{6}Li, ^{10}Be → ^{10}B, and ^{14}C → ^{14}N calculated by $T\beta\gamma$-AMD+GCM.

as leading components in particular in light nuclei. As the mass number increases, the LS-coupling $T=1,S=0$ NN pairs are somewhat broken into jj-coupling pairs because of the spin-orbit mean potential. We can see this systematics especially in $\langle \boldsymbol{S}^2\rangle$ for the $0_1{}^+1$ states. ^{6}He($0_1{}^+1$) has almost pure $S=0$ component with only 6% mixing of $S=1$ component estimated from $\langle \boldsymbol{S}^2\rangle=0.12$. However, ^{14}C($0_1{}^+1$) has a broken $S=0$ two-hole pair with significant $S=1$ component up to 27%. In contrast to the $T=1$ states, the LS-coupling pn pairs in the $T=0$ states is not broken; the $S=0$ mixing is found to be less than 6% for all the $T=0$ states. This result implies that $T=0,S=1$ pn pairs are robuster than $T=1,S=0$ NN pairs.

For the orbital angular momentum, values of $\langle \boldsymbol{L}^2\rangle\approx 0$ and $\langle \boldsymbol{L}^2\rangle\approx 6$ indicate dominant $L=0$ and $L=2$ components, respectively. In $A=6$ nuclei, the total orbital angular momentum L is contributed only by the orbital angular momentum L_{NN} of the NN pair because the α core is spherical. Therefore, the ground states ^{6}He($0_1{}^+1$) and ^{6}Li($1_1{}^+0$) are understood well by $S=0,T=1$ and $S=1,T=0$ NN pairs moving around the α in $L_{NN}=0$ wave, whereas the excited states ^{6}He($2_1{}^+1$) and ^{6}Li($1_2{}^+0,2_1{}^+0,3_1{}^+0$) contain $S=0,T=1$ and $S=1,T=0$ NN pairs in $L_{NN}=2$ wave. Also for the $A=14$ systems, the dominant components of ^{14}C($0_1{}^+1$) and ^{14}N($1_2{}^+1$) have two holes in the spherical ^{16}O core coupled to be $S=0,T=1$ and $S=1,T=0$ pairs in $L_{NN}=0$ wave, whereas those of ^{14}C($2_1{}^+1$) and ^{14}N($1_1{}^+0,2_1{}^+0,3_1{}^+0$) are understood by $S=0,T=1$ and $S=1,T=0$ two-hole pairs in $L_{NN}=2$ wave.

Based on LS-coupling of NN pairs, we can easily understand spin-isospin partners and their strong GT transitions. The GT operator changes intrinsic spin configuration with $\Delta S=1$ from $T=1$ states to $T=0$ states but it does not affect orbital configurations. In the case of $L_{\rm core}=0$, nn pairs in $[L_{NN}=0,S_{NN}=0]_{J=0}$ initial states change directly into $T=0$ pn pairs in $[L_{NN}=0,S_{NN}=1]_{J=1}$ states with strengths of the sum rule value: $\sum_n B({\rm GT};0^+1\to 1_n^+0)=6$ provided that core nuclei are spin-isospin saturated states and do not contribute to the GT transitions. Similarly, we can easily understand the spin-isospin partners of $[L_{NN}=2,S_{NN}=0]_{J=2}$ initial states and $[L_{NN}=2,S_{NN}=1]_{J=1,2,3}$ final states. Although J in the final states is not unique because of angular momentum coupling of $S_{NN}=1$ with nonzero L_{NN}, we can again obtain the sum rule: $\sum_{J=1,2,3}\sum_n B({\rm GT};2^+1\to J_n^+0)=6$. It should be pointed out that, since $S=1$ pn pairs in $L_{NN}=2$ wave feel spin-orbit mean potentials from core nuclei, energy spectra of the final $J=1,2,3$ states show spin-orbit splitting which plays an essential role in lowering the $T=0$ states into the ground states in ^{10}B and ^{14}N.

If the NN pairs are broken into jj-coupling pairs, the concentration of GT transition strengths does not occur because initial states change into various (jj') configurations. In other words, the concentration of GT transition strengths to specific final states is a good measure for realization of LS-coupling NN pairs. Based on the LS-coupling picture of NN pairs, we assigned the spin-isospin partners for $T=1$ states and $T=0$ states with strong GT transition strengths which are qualitatively characterized by $\Delta T=0$, $\Delta S=1$, $\Delta L=0$ transitions.

Figure 3 shows the calculated energy spectra and the GT transitions for the spin-isospin partners in $A=6$, $A=10$, and $A=14$. The GT transition from ^{6}He($0_1{}^+1$) to ^{6}Li($1_1{}^+0$) is enhanced because these states have the same $L_{NN}=0$ nature. For the excited states, the GT transitions from ^{6}He($2_1{}^+1$) to ^{6}Li($1_2{}^+0,2_1{}^+0,3_1{}^+0$) are strong because of the transition from the $T=1,S=0$ pair to the $T=0,S=1$ pair in the dominant $L_{NN}=2$ component. The sum of the GT strengths from ^{6}He($2_1{}^+1$) exhausts a large fraction of the sum rule value, indicating that the nature of spin-isospin partners still remains also in the excited states. In the energy spectra of

^{6}Li($1_2^+0, 2_1^+0, 3_1^+0$), the ordering of 3_1^+0, 2_1^+0, and 1_2^+0 is easily understood by the spin-orbit splitting for the $S = 1$ pn pairs in $L_{NN} = 2$.

In ^{14}N spectra, low-lying states are understood as spin-isospin partners of ^{14}C for NN hole pairs in the spherical ^{16}O core. ^{14}C(0_1^+1) has a strong GT transition not to the lowest 1^+0 state but to the excited 1^+0 state, ^{14}N(1_2^+0) because these states have NN hole pairs in the same $L_{NN} = 0$ orbit. Then, the GT transition occurs from the $S = 0$ pp hole pair to the $S = 1$ pn hole pair. The GT transitions from ^{14}C(2_1^+1) to ^{14}N($1_1^+0, 2_1^+0, 3_1^+0$) show spin-isospin-flip features of NN hole pairs. Indeed, ^{14}N($1_1^+0, 2_1^+0, 3_1^+0$) spectra show the spin-orbit splitting of the $S = 1$ pn hole pairs in $L_{NN} = 2$. Note that the ordering 1_1^+0, 2_1^+0, and 3_1^+0 is opposite to that of the particle-particle pair case because the spin-orbit mean potentials for hole states are repulsive.

Our assignments are consistent with the strong GT transition for ^{14}C(0_1^+1) $\rightarrow$ ^{14}N(1_2^+0) experimentally measured by charge exchange reactions. Moreover, for the transitions from ^{14}N(1_1^+0), relatively strong GT transitions to ^{14}C(2_1^+1) and ^{14}C(2_2^+1) have been observed by charge exchange reactions [29]. They support a significant $L_{NN} = 2$ component in ^{14}N(1_1^+0), consistent with the present assignment, though quantitative reproduction of the B(GT) values is not satisfactory in the present calculation.

For the GT transition between the ground states of ^{14}C and ^{14}N, the experimental B(GT; ^{14}C(0_1^+1) $\rightarrow$ ^{14}N(1_1^+0)) is anomalously small, known as a long life problem of ^{14}C. The suppression of the GT transition of ^{14}C(0_1^+1) $\rightarrow$ ^{14}N(1_1^+0) is partially understood by the NN pair picture in LS coupling that ^{14}N(1_1^+0) is the spin-isospin partner not of the ^{14}C(0_1^+1) but of ^{14}C(2_1^+1), because of the large spin-orbit splitting for the $S = 1$ pn hole pairs in $L_{NN} = 2$. It is different from the $A = 6$ and $A = 10$ systems, in which the lowest 1^+0 state is the spin-isospin partner of the ground state of the $N = Z + 2$ nucleus. The GT transition from the $[L_{NN} = 0, S_{NN} = 0]_{J=0}$ component in ^{14}C(0_1^+1) to the $[L_{NN} = 2, S_{NN} = 1]_{J=1}$ component in ^{14}N(1_1^+0) is forbidden because of the difference $\Delta L_{NN} = 2$ in spatial configurations. In other words, the GT transition is suppressed because of the LS-coupling pair correlation. Indeed, the calculated B(GT) = 0.30 is factor 1 smaller than the sum rule value and less than half of the jj-coupling limit B(GT) = 2/3 for the pure $p_{1/2}^{-2}$ configuration without the pair correlation. Our result for B(GT; ^{14}C(0_1^+1) $\rightarrow$ ^{14}N(1_1^+0)) is the same order as those of a NCSM calculation [12] and AMD+VAP calculation [33] but still largely overestimates the experimental data. In the present calculation, the NN pairs in ^{14}C(0_1^+1) and ^{14}N(1_1^+0) dominantly have $[L_{NN} = 0, S_{NN} = 0]_{J=0}$ and $[L_{NN} = 2, S_{NN} = 1]_{J=1}$ components, respectively, but they are not necessarily ideal LS-coupling pairs. Moreover, $[L_{NN} = 2, S_{NN} = 1]_{J=1}$ and $[L_{NN} = 0, S_{NN} = 1]_{J=1}$ are somewhat mixed with each other in the obtained ^{14}N(1_1^+0) and ^{14}N(1_2^+0). As a result of significant mixing of configurations, the calculated GT transition ^{14}C(0_1^+1) $\rightarrow$ ^{14}N(1_1^+0) does not vanish. Additional scenarios are required to solve the long-life problem of ^{14}C(0_1^+1). Traditionally, it is understood as accidental cancellation of matrix elements because of the tensor force [15]. Recently, the NCSM calculation [12] has also reproduced the long lifetime by fine tuning of the three-body force in chiral perturbation theory. In both cases, phenomenological adjustment of the original interactions is needed to fit the GT transition for ^{14}C(0_1^+1) and ^{14}N(1_1^+0).

In the above cases of $A = 6$ and $A = 14$ nuclei, the core nuclei, α and ^{16}O, have almost spherical shapes for both ground and excited states. In the $A = 10$ nuclei, on the other hand, not only L_{NN} but also $L_{\rm core}$ from collective rotation of the deformed core contributes to L. Consequently, two types of spin-isospin partners corresponding to $L_{NN} = 2$ and $L_{\rm core} = 2$ are found in the low-lying spectra of ^{10}B. Namely, we should also consider the spin-isospin partners of $[L_{\rm core} = 2, L_{NN} = 0, S_{NN} = 0]_{J=2}$ initial states and $[L_{\rm core} = 2, L_{NN} = 0, S_{NN} = 1]_{J=1,2,3}$ final states in addition to the transition from $[L_{NN} = 0, S_{NN} = 0]_{J=0}$ to $[L_{NN} = 0, S_{NN} = 0]_{J=1}$ and those from $[L_{NN} = 2, S_{NN} = 0]_{J=2}$ to $[L_{NN} = 2, S_{NN} = 0]_{J=1,2,3}$, which we have already discussed for $A = 6$ and $A = 14$ nuclei.

For ^{10}Be(0_1^+1) and ^{10}B(1_1^+0), $\langle \boldsymbol{L}^2 \rangle \approx 0$ indicates that these states can be approximately described by the $S = 0, T = 1$ and $S = 1, T = 0$ NN pairs with $L_{NN} = L_{\rm core} = 0$. The orbital angular momentum $L \approx 2$ of ^{10}Be(2_1^+1) mainly comes from the core rotation $L_{\rm core} = 2$, whereas that of ^{10}Be(2_2^+1) is contributed mainly by $L_{NN} = 2$ from the NN pair rotation because the former and the latter states are a member of the $K = 0$ ground band and that of the $K = 2$ side band, respectively. It means that ^{10}Be(0_1^+1) and ^{10}Be(2_2^+1) are described by $S = 0$ nn pairs in $L_{NN} = 0$ and $L_{NN} = 2$ waves, respectively, and ^{10}Be(2_1^+1) is understood by an $S = 0$ nn pair with collective rotation ($L_{\rm core} = 2$). The corresponding spin-isospin partners in ^{10}B should have $S = 1, T = 0$ pn pairs with consistent spatial configurations.

We can also understand the GT transition from ^{10}Be(0_1^+1) to ^{10}B(1_1^+0) in the picture of LS-coupling NN pairs as a GT transition from a nn pair to a $T = 0$ pn pair in $L_{NN} = 0$. For the excited states ^{10}Be(2_1^+1) and ^{10}Be(2_2^+1), two sets of $J^\pi = \{1^+, 2^+, 3^+\}$ for the spin-isospin partners appear in the $T = 0$ spectra, but the 2^+0 states are strongly mixed with each other because they almost degenerate energetically. ^{10}Be(2_1^+1) has a rotating core with $L_{\rm core} = 2$ and it has strong transition strength to ^{10}B($1_2^+0, 2_{1,2}^+0, 3_2^+0$), which almost degenerates because there is no spin-orbit splitting for the $T = 0$ pn pairs in $[L_{\rm core} = 2, L_{NN} = 0, S_{NN} = 1]_{J=1,2,3}$. ^{10}Be($2_2^+1$) with a rotating $S = 0$ nn pair in $L_{NN} = 2$ has a dominant transition strength to ^{10}B($1_3^+0, 2_{1,2}^+0, 3_1^+0$), which shows large spin-orbit splitting of the $S = 1$ pn pairs in $L_{NN} = 2$. As a result of the spin-orbit splitting, the 3^+0 state partnered with ^{10}Be(2_2^+1) comes down to the ground state of ^{10}B. This assignment is consistent with the experimental data of the strong GT transition for ^{10}B(3_1^+0) $\rightarrow$ ^{10}Be(2_2^+1) measured by charge exchange reactions [30]. Strictly speaking, it is in principle unable to definitely define $L_{\rm core}$ and L_{NN} for $N = Z$ odd-odd nuclei with deformed cores because core nucleons and valence nucleons are identical fermions and are indistinguishable in fully microscopic wave functions of identical fermions. Nevertheless, the GT transitions from $N = Z + 2$ neighbors are observables, and they enable us to classify the final states in $T = 0$ $N = Z$ odd-odd nuclei in terms of $T = 0$ pn pairs in connection with nn pairs in the initial states of $N = Z + 2$ nuclei.

Similar discussions have been given in works with shell model calculations for ^{10}B to understand $M1$ transitions from isobaric analog states in ^{10}B [4,5] instead of the GT transitions from ^{10}Be. In Ref. [4], the $M1$ transitions between $T = 0$ and $T = 1$ states of ^{10}B are described well by SU(4)-supermultiplet theory, in which strong transitions of $0_1^+1 \to 1_1^+0$, $2_1^+1 \to 1_2^+0$, $2_1^+1 \to 2_1^+0$, and $2_2^+1 \to 3_1^+0$ and weak ones of $2_1^+1 \to 1_1^+0$ and $2_1^+1 \to 3_1^+0$ can be understood from the point of view of L- and K_L-selection rules. The feature of the $M1$ transitions shows good correspondence to that of the GT transitions, and the discussion in Ref. [4] based on the SU(4)-supermultiplet theory in the p shell is, in a sense, analogous to the present discussion of the spin-isospin flip partners for the GT transitions. However, as mentioned previously, the obtained wave functions contain significant higher shell components (see Table III) beyond the p shell because of the spatial development of two-nucleon pairs as well as that of the 2α cluster, and therefore we cannot apply the strong-coupling picture within the p-shell configuration.

In the present analysis, we can understand low-energy spectra of $A = 6$, $A = 10$, and $A = 14$ nuclei from the LS-coupling NN pair picture and assign spin-isospin partners not only for the 0^+1 initial states but also the 2^+1 initial states as shown in Fig. 3. The spin-orbit splitting of the $J^\pi T = 1^+0,2^+0,3^+0$ states with $L_{NN} = 2$ coupled with the intrinsic spin $S = 1$ of the NN pair is essential in the spectra of $N = Z$ odd-odd nuclei. In the systematics of the spin-orbit splitting shown in Fig. 3, we can see that the splitting becomes large as A increases. It implies that the LS-coupling NN pairs feel the stronger spin-orbit mean potential in heavier systems.

V. SUMMARY AND OUTLOOK

We have studied the Gamow-Teller transitions from $N = Z + 2$ neighbors to $N = Z$ odd-odd nuclei in the p-shell region by using $T\beta\gamma$-AMD+GCM. We have obtained that the strong GT transitions exhaust more than 50% of the sum rule for ^{6}He$(0_1^+1) \to {}^6$Li(1_1^+0), ^{10}Be$(0_1^+1) \to {}^{10}$B(1_1^+0), and ^{14}C$(0_1^+1) \to {}^{14}$N(1_2^+0). We have also found the concentration of the GT strengths of the transitions from 2_1^+1 states, ^{6}He$(2_1^+1) \to {}^6$Li$(1_2^+0,2_1^+0,3_1^+0)$, ^{10}Be$(2_1^+1) \to {}^{10}$B$(1_2^+0,2_1^+0,2_2^+0,3_2^+0)$, ^{10}Be$(2_2^+1) \to {}^{10}B(1_3^+0,2_1^+0,2_2^+0,3_1^+0)$, and ^{14}C$(2_1^+1) \to {}^{14}N(1_1^+0,2_1^+0,3_1^+0)$. These states connected with the strong GT transitions can be interpreted as "spin-isospin partner" states.

For further analysis, we have introduced two-nucleon-pair densities to see spatial development of the NN pairs around the α, 2α, and ^{12}C cores for $A = 6$, $A = 10$, and $A = 14$ nuclei. We have found that $S = 0, T = 1$ nn pairs and $S = 1, T = 0$ pn pairs are dominantly formed in the $N = Z + 2$ and $N = Z$ odd-odd nuclei, respectively. Systematically, the $T = 0$ pn pairs more remarkably develop away from the core nuclei than the nn pairs do.

In ^{10}Be, ^{10}B, we have found the largely deformed core because of spatial development of the 2α structure. It contributes to better reproduction of the $E2$ and Q moment values than those of shell-model calculations. From the collective rotation of the deformed core and NN pairs, the rotational and side bands are constructed in the low-lying spectra as the ground band of ^{10}Be(0_1^+1) and ^{10}Be(2_1^+1) and the side band of ^{10}Be(2_2^+1). Because of the spatial development of the NN pairs and the core deformation, ^{10}Be and ^{10}B states contain significantly higher shell components beyond p-shell as shown in their large $\Delta\mathcal{N}_{\hbar\omega}$ values.

The GT transitions is a good probe to clarify the dynamics of the pn pairs in $N = Z$ odd-odd nuclei through the connection with the nn pairs in the neighboring nuclei. From such a point of view, we have studied the spin and orbital configurations of the LS-coupling NN pairs and discussed the behaviors of the LS-coupling NN pairs in relation to the GT transitions. The ground states of $N = Z + 2$ nuclei, ^{6}He(0_1^+1), ^{10}Be(0_1^+1), and ^{14}C(0_1^+1), and their partner states, ^{6}Li(1_1^+0), ^{10}B(1_1^+0), and ^{14}N(1_2^+0), have major $L = 0$ components, in which both the NN pairs and the core nuclei are in $L = 0$ states. The excited states, ^{6}He(2_1^+1), ^{10}Be(2_2^+1), and ^{14}C(2_1^+1), and their partner states have dominantly $L = 2$ components mainly contributed by the NN rotation around the core, whereas ^{10}Be(2_1^+1) and its spin-isospin partners have $L = 2$ components with the deformed 2α core rotating in $L = 2$.

Based on the LS-coupling NN pairs, the strong GT transitions between spin-isospin partners can be understood as spin-isospin-flip phenomena from the $S = 0, T = 1$ nn pairs in the $N = Z + 2$ initial states to $S = 1, T = 0$ pn pairs in the $N = Z$ odd-odd final states. Namely, the transitions ^{6}He$(0_1^+1) \to {}^6$Li(1_1^+0), ^{10}Be$(0_1^+1) \to {}^{10}$B(1_1^+0) and ^{14}C$(0_1^+1) \to {}^{14}$N(1_2^+0) are spin-flip phenomena of the NN pairs with $[L_{\rm core} = 0, L_{NN} = 0]_{L=0}$, whereas ^{6}He$(2_1^+1) \to {}^6Li(1_2^+0,2_1^+0,3_1^+0)$, ^{10}Be$(2_2^+1) \to {}^{10}B(1_3^+0,2_1^+0,2_2^+0,3_1^+0)$, and ^{14}C$(2_1^+1) \to {}^{14}N(1_1^+0,2_1^+0,3_1^+0)$ are those with $[L_{\rm core} = 0, L_{NN} = 2]_{L=2}$.

In the latter cases, the spectra of three final states with $J^\pi = 1^+,2^+,3^+$ are split because of the spin-orbit interaction for the $S = 1, T = 0$ pn pairs in the $L_{NN} = 2$ wave. The spin-orbit splitting describes $J \geqslant 1$ of the ground states in $N = Z$ odd-odd nuclei except for the case of two nucleons around a magic number core. On the other hand, the spectra of ^{10}B$(1_2^+0,2_1^+0,2_2^+0,3_2^+0)$ partnered with ^{10}Be(2_1^+1) show small splitting because these states have a dominant $[L_{\rm core} = 2, L_{NN} = 0]_{L=2}$ component, in which the spin-orbit interaction does not affect the $S = 1, T = 0$ pn pairs in the $L_{NN} = 0$ wave.

In comparison with experimental data, the magnetic moments μ and the magnetic dipole transition strengths $B(M1)$ are reasonably reproduced in the present calculation. Moreover, relatively enhanced B(GT) for ^{6}He$(0_1^+1) \to {}^6$Li(1_1^+0), ^{10}Be$(0_1^+1) \to {}^{10}$B(1_1^+0), and ^{14}C$(0_1^+1) \to {}^{14}$N(1_2^+0) show features consistent with the present results. The present calculation also succeeds in describing the concentrations of the GT strengths from the $J = 2$ excited states: ^{10}Be$(2_2^+1) \to {}^{10}$B(3_1^+0) and ^{14}C$(2_1^+1) \to {}^{14}$N(1_1^+0).

We have also compared our results with shell-model ones. μ, $B(M1)$, and B(GT) values have shown similar nature; however, Q and $B(E2)$ of ^{10}B are much improved. It indicates the advantage of our method, $T\beta\gamma$-AMD+GCM, in describing the spatial developments of pn pair and core deformation originating from clusterizations in the same footing. However,

we should comment that the anomalous suppression of the GT transition $^{14}C(0_1{}^+1) \rightarrow {}^{14}N(1_1{}^+0)$ is not reproduced in our calculation. Fine tuning of the interaction should be needed to reproduce this value, as discussed in many works.

Our calculation generally overestimates the strong GT transitions in $A = 10$ and $A = 14$ by about a factor 1.5. A possible reason for the overestimations might be omission of higher order correlations such as short-range and tensor correlations in the present model space. To overcome this problem, a more sophisticated structure model which can explicitly take into account such higher order correlations may be required.

In light nuclei, the LS-coupling pn pairs are formed. However, for heavier nuclei, the description of pn pair correlation in LS coupling is no longer valid because jj-coupling pn pairs and also the pn pair condensation are expected because of the spin-orbit interactions. Further investigations of $N = Z$ odd-odd nuclei in a wide mass number region from light to heavy mass nuclei are required for deeper understanding of pn pair correlations.

ACKNOWLEDGMENTS

The computational calculations of this work were performed using the supercomputers in the Yukawa Institute for theoretical physics, Kyoto University. This work was supported by JSPS KAKENHI Grants No. 16J05659 and No. 26400270.

[1] S. Frauendorf and A. O. Macchiavelli, Prog. Part. Nucl. Phys. **78**, 24 (2014).
[2] Y. Tanimura, H. Sagawa, and K. Hagino, Prog. Theor. Exp. Phys. **2014**, 53D02 (2014).
[3] H. Morita and Y. Kanada-En'yo, Prog. Theor. Exp. Phys. **2016**, 103D02 (2016).
[4] D. Kurath, Nucl. Phys. A **317**, 175 (1979).
[5] F. C. Barker, Aust. J. Phys. **34**, 7 (1981).
[6] Y. Fujita *et al.*, Phys. Rev. C **91**, 064316 (2015).
[7] A. Gezerlis, G. F. Bertsch, and Y. L. Luo, Phys. Rev. Lett. **106**, 252502 (2011).
[8] B. Cederwall *et al.*, Nature (London) **469**, 68 (2011).
[9] C. Qi, J. Blomqvist, T. Bäck, B. Cederwall, A. Johnson, R. J. Liotta, and R. Wyss, Phys. Rev. C **84**, 021301(R) (2011).
[10] H. Wolter, A. Faessler, and P. Sauer, Nucl. Phys. A **167**, 108 (1971).
[11] K. Yoshida, Phys. Rev. C **90**, 031303(R) (2014).
[12] P. Maris, J. P. Vary, P. Navrátil, W. E. Ormand, H. Nam, and D. J. Dean, Phys. Rev. Lett. **106**, 202502 (2011).
[13] P. Navrátil and W. E. Ormand, Phys. Rev. C **68**, 034305 (2003).
[14] W.-T. Chou, E. K. Warburton, and B. A. Brown, Phys. Rev. C **47**, 163 (1993).
[15] B. Jancovici and I. Talmi, Phys. Rev. **95**, 289 (1954).
[16] T. Suhara and Y. Kanada-Enyo, Prog. Theor. Phys. **123**, 303 (2010).
[17] N. Itagaki, T. Otsuka, K. Ikeda, and S. Okabe, Phys. Rev. Lett. **92**, 142501 (2004).
[18] N. Itagaki, S. Okabe, K. Ikeda, and I. Tanihata, Phys. Rev. C **64**, 014301 (2001).
[19] S. Okabe and Y. Abe, Prog. Theor. Phys. **61**, 1049 (1979).
[20] N. Itagaki and S. Okabe, Phys. Rev. C **61**, 044306 (2000).
[21] T. Suhara and Y. Kanada-Enyo, Phys. Rev. C **82**, 044301 (2010).
[22] D. R. Tilley, C. M. Cheves, J. L. Godwin, G. M. Hale, H. M. Hofmann, J. H. Kelley, C. G. Sheu, and H. R. Weller, Nucl. Phys. A **708**, 3 (2002).
[23] D. R. Tilley, J. H. Kelley, J. L. Godwin, D. J. Millener, J. E. Purcell, C. G. Sheu, and H. R. Weller, Nucl. Phys. A **745**, 155 (2004).
[24] F. Ajzenberg-Selove, Nucl. Phys. A **523**, 1 (1991).
[25] W. M. Visscher and R. A. Ferrell, Phys. Rev. **107**, 781 (1957).
[26] M. S. Fayache, L. Zamick, and H. Muther, Phys. Rev. C **60**, 067305 (1999).
[27] J. W. Holt, G. E. Brown, T. T. S. Kuo, J. D. Holt, and R. Machleidt, Phys. Rev. Lett. **100**, 062501 (2008).
[28] J. W. Holt, N. Kaiser, and W. Weise, Phys. Rev. C **81**, 024002 (2010).
[29] F. Ajzenberg-Selove, Nucl. Phys. A **490**, 1 (1988).
[30] I. Daito *et al.*, Phys. Lett. B **418**, 27 (1998).
[31] A. Negret, T. Adachi, B. R. Barrett, C. Baumer, A. M. van den Berg, G. P. A. Berg, P. von Brentano, D. Frekers *et al.*, Phys. Rev. Lett. **97**, 062502 (2006).
[32] J. Rapaport, P. W. Lisowski, J. L. Ullmann, R. C. Byrd, T. A. Carey, J. B. McClelland, L. J. Rybarcyk, T. N. Taddeucci, R. C. Haight, N. S. P. King, G. L. Morgan, D. A. Clark, D. E. Ciskowski, D. A. Lind, R. Smythe, C. D. Zafiratos, D. Prout, E. R. Sugarbaker, D. Marchlenski, W. P. Alford, and W. G. Love, Phys. Rev. C **39**, 1929 (1989).
[33] Y. Kanada-En'yo and T. Suhara, Phys. Rev. C **89**, 044313 (2014).